Growth and structural transition of Fe ultrathin films on Ni(111) investigated by LEED and STM

Bai An, Lin Zhang, Seiji Fukuyama, and Kiyoshi Yokogawa
National Institute of Advanced Industrial Science and Technology (AIST), Central 5, 1-1-1 Higashi, Tsukuba, Ibaraki 305-8565, Japan
(Received 23 July 2008; revised manuscript received 9 January 2009; published 5 February 2009)

The growth of Fe ultrathin films on Ni(111) at room temperature has been investigated by low-energy electron diffraction and scanning tunneling microscopy. In the initial deposition, a pseudomorphic fcc-Fe(111) monolayer with triangular line defects grows on the Ni substrate. Triangular lines consist of atomic-size dark spots located in the Ni atom sites and are interpreted in terms of the misfit-induced atomic vacancies in the Ni substrate. With further deposition, the second monolayer Fe film, which consists of three elongated domains of a striped structure, grows on the first monolayer fcc-Fe film. The striped structure results from the growth of a distorted bcc-Fe(110) phase with one-dimensional Nishiyama-Wassermann orientation. Further deposition leads to the growth of thicker bcc (110) films on the distorted bcc(110) domains, forming three-dimensional ridgelike islands. The first and second monolayer Fe films grow in an incomplete layer-by-layer growth mode and the thicker Fe films grow in a three-dimensional island growth mode.

DOI: 10.1103/PhysRevB.79.085406 PACS number(s): 68.55.−a, 68.37.Ef, 81.15.Np, 64.70.K−

I. INTRODUCTION

Since theoretical calculations[1,2] showed that fcc γ-iron (γ-Fe), which do not exist below 1185 K in bulk but can exist at room temperature (RT) in thin epitaxial films grown on suitable fcc substrates,[3] may be nonmagnetic, antiferromagnetic, and ferromagnetic depending on lattice parameters, the growth of Fe ultrathin films on fcc substrates has been extensively studied.[3–20] Copper (Cu) single crystal has been the most widely used substrate[3–7] because its lattice parameter (3.61 Å) is near that of fcc-Fe at RT (3.59 Å) and it is nonmagnetic, which allows us to single out the magnetic properties of the Fe film.[8] However, it has been recently found that the bcc-like structure coexists with the fcc structure from the initial stage of Fe film growth on the Cu substrates,[9–11] which throws doubt on the established ferromagnetic fcc model in this prototypical system.[10,11]

Nickel (Ni) is also a suitable substrate, as far as the lattice mismatch is concerned (3.52 Å), and in principle could be a better substrate for the layer-by-layer growth of Fe because its surface free energy is higher than that of Cu.[12,13] Moreover, the use of Ni instead of Cu as a substrate adds interest and complexity to the system since Ni is ferromagnetic and its magnetic moment influences the magnetic moment of the Fe film.[14,15] Thus, the growth of Fe ultrathin films on Ni has also been investigated by many surface analysis techniques.[13,15–20] Luches and co-workers[15,16] investigated the structures of Fe thin films grown on Ni(001) single crystal by primary-beam-diffraction-modulated electron emission and photoelectron diffraction (PD) and concluded that, within the first five monolayer (ML), the Fe film was fcc(001) and intermixing with the substrate extended over the first three ML. At a higher Fe coverage, a transition to the bcc(110) phase was suggested.[15,16] D'Addato *et al.*[13] observed the growth of Fe ultrathin films on Ni(111) single crystal by low-energy electron diffraction (LEED) and electron energy-loss spectroscopy (EELS), and interpreted that a phase transition from fcc(111) to bcc(110) with the Kurdjumov-Sachs (KS) orientation occurred in 4 ML Fe films. Gazzadi *et al.*[17] investigated the structures of Fe thin films grown on Ni(111) single crystal by angle-scanned PD and quantitative analysis, and found that the Fe atoms in the first monolayer occupied the fcc hollow sites of the Ni(111) substrate and were stacked with a pseudomorphic fcc structure up to 2 ML. Between 3 and 6 ML, a transition to the bcc(110) phase with the Nishiyama-Wassermann (NW) orientation was induced.[17] They considered that the previous erroneous interpretation about the KS orientation of the bcc(110) (Ref. 13) was due to the poor quality and misorientation of the LEED pattern. Johnston *et al.*[18] studied the growth of Fe films on 2 ML Ni/W(110) substrate by LEED and angle-resolved Auger-electron spectroscopy (AES). They observed that a slightly distorted fcc(111) structure grew up to 3 ML, and then, a complex transition to the bcc(110) phase involving both the KS and NW orientations developed with increasing thickness.[18] Sander *et al.*[19] observed the Fe ultrathin films grown on 2 ML-Ni/W(110) with a coverage of 0.8 ML by scanning tunneling microscopy (STM). They found that the Fe films consisted of monolayer Fe islands with small second-layer Fe islands. However, they did not present the STM results on the Fe films thicker than 0.8 ML. Therefore, the thickness dependence of the morphology and atomic structure of the Fe ultrathin films on Ni substrates has not yet been demonstrated in real space.

Recently, the present authors have observed the epitaxial growth of an Fe monolayer on a Ni(111) single crystal by STM and found that triangular line defects consisting of dark spots were formed on the Fe monolayer and reconstructed by hydrogen adsorption.[20]

In the present study, we systematically investigate the growth of Fe ultrathin films on Ni(111) single crystal at RT up to an average coverage of 4.5 ML, by combined LEED and STM, in order to characterize the morphology and atomic structures of the Fe ultrathin films growing on the Ni(111) single crystal.

II. EXPERIMENT

Experiments were performed in an ultrahigh-vacuum (UHV) system equipped with devices for LEED, AES, and

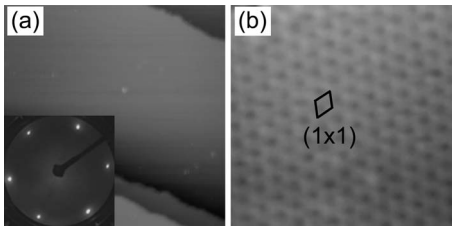

FIG. 1. STM images of clean Ni(111) surface. (a) Large-scale image (50×50 nm^2). The inset shows the corresponding LEED pattern (85 eV). (b) Atomic image (3×3 nm^2).

STM. The base pressure of the system was below 7×10^{-9} Pa. A Ni(111) single crystal with a purity of 99.9999% and dimensions of $2\times2\times0.3$ mm^3 was mounted on a sheet holder made of tantalum with a thickness of 0.04 mm, which resistively heats the specimen to 1500 K, and was cleaned by repeated Ar ion sputtering and heating at 1200 K in the UHV system. The temperature of Ni(111) was measured using an optical pyrometer set outside the UHV chamber. Figure 1 shows the STM images of a clean Ni(111) surface prepared by Ar ion sputtering and heating in the UHV chamber. Flat terraces separated by atomic steps are observed on the surface, as shown in Fig. 1(a), and the well-ordered atoms reflecting the sixfold symmetry of the substrate surface are observed on these terraces, as shown in Fig. 1(b). The corresponding LEED pattern shows very sharp (1×1) spots, which is in agreement with the STM image, as shown in the inset in Fig. 1(a).

Fe ultrathin films were grown on Ni(111) at RT by evaporating a pure Fe wire of 99.999% purity from a distance of 100 mm. The deposition rate, which was determined by STM coverage measurement in a submonolayer region, was about 0.6 ML min^{-1}.

STM images were obtained at room temperature in the UHV chamber. A tungsten rod sharpened by electrochemical etching in KOH solution was used as the STM tip. Additionally, electron bombardment was applied to clean the STM tip in the UHV chamber before measurement. STM measurements were performed in the constant-current mode with a tip bias of 0.02–0.5 V and a tunneling current of 0.4–8 nA.

III. RESULTS

Figure 2 shows the STM images obtained from Fe films with an Fe coverage of 0.66 ML. In the large-scale STM image shown in Fig. 2(a), monolayer Fe films grow from the step edges of the Ni(111) substrate, and a monolayer Fe island grows on the large terrace of the Ni(111) substrate. The monolayer Fe film wetted at the Ni step edge appears to be brighter than the Ni terrace. The LEED pattern still shows the (1×1) spots similar to those of the clean Ni(111) surface, as shown in the inset in Fig. 2(a), indicating the epitaxial growth of a pseudomorphic fcc structure on Ni(111). It is also observed that the equilateral triangles composed of thin depression lines of 2–5 nm side length are formed on the monolayer Fe films, as reported in our recent study.[20] The depression lines of the triangles consist of aligned dark spots with a spacing of 0.5 nm along the $\langle1\bar{1}0\rangle$ direction, as shown

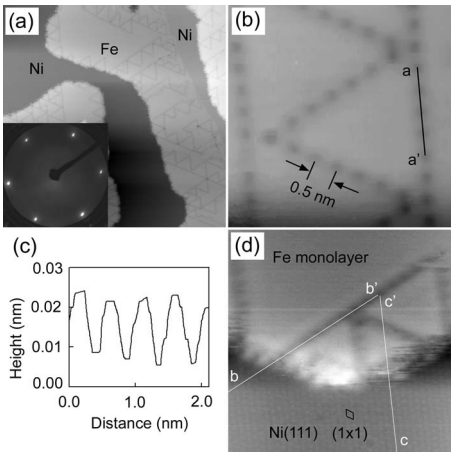

FIG. 2. STM images of Fe films grown on Ni(111) with Fe coverage of 0.66 ML. (a) Large-scale image (60×60 nm^2). The inset shows the corresponding LEED pattern (85 eV). (b) Magnified image (5×5 nm^2) of triangular line defects composed of dark spots. (c) Cross-sectional line profile taken along line aa' in (b). (d) Magnified image (8×8 nm^2) of first monolayer Fe film and Ni substrate.

in the magnified image in Fig. 2(b). The cross-sectional line profile taken along the line aa', which is drawn through the dark spots in the image, is shown in Fig. 2(c), from which the depths of the dark spots are measured to be less than 0.03 nm. Figure 2(d) shows another high-resolution STM image, where both the (1×1) structure of the Ni substrate and the Fe island with the triangular lines consisting of dark spots are visible. Two white lines bb' and cc' are drawn through the Ni atoms arranged along two $\langle1\bar{1}0\rangle$ directions in the image. The intersection point of the two lines is located on a dark spot, indicating that the dark spot is located in a Ni atom site. Since the distance of 0.5 nm between dark spots is just twice the interatomic distance of the Ni(111) plane along the $\langle1\bar{1}0\rangle$ direction, the dark spots are located in every second Ni atom site along the $\langle1\bar{1}0\rangle$ direction.

With increasing deposition up to about 0.72 ML, the second monolayer Fe films begin to grow on the first monolayer Fe films. Figure 3 shows the STM images obtained from Fe films with an Fe coverage of 1.2 ML. The first monolayer Fe films grow over an area of approximately 86% on the substrate surface and the second monolayer Fe films grow over an area of approximately 39% on the first monolayer Fe films, as shown in the large-scale image in Fig. 3(a), where the second monolayer Fe films are outlined by dotted lines. It is observed that the second monolayer Fe films tend to grow along the $\langle1\bar{1}0\rangle$ direction with elongated shapes, as indicated by arrows in the image. A high-resolution STM image of a second monolayer Fe film island with a small patch of a third monolayer Fe film is shown in Fig. 3(b). The three domains of the striped structure are observed on the second monolayer Fe film island. The domains are outlined by dotted lines, and the stripes that run perpendicular to the $\langle1\bar{1}0\rangle$ direction are indicated by parallel lines on each domain. The periodic distance between the stripes is approximately 1.8 nm. We call these large stripes as long-period stripes. The

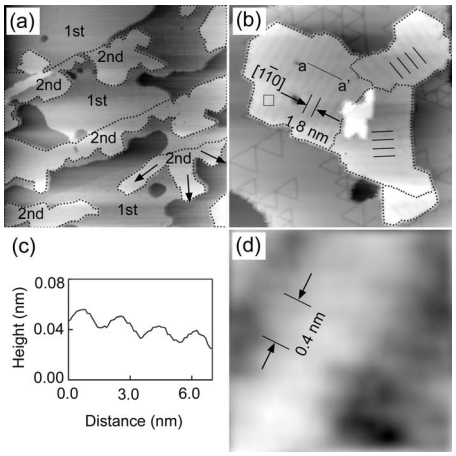

FIG. 3. STM images of Fe films grown on Ni(111) with Fe coverage of 1.2 ML. (a) Large-scale image (153×153 nm^2). (b) Magnified image (40×40 nm^2) of second monolayer Fe film. (c) Cross-sectional line profile taken along line aa' in (b). (d) Magnified image (2.3×2.3 nm^2) of the square area indicated in (b).

cross-sectional line profile taken along the line aa' in (b) indicates that the corrugation of the long-period stripes is approximately 0.01 nm, as shown in Fig. 3(c). Along each long-period stripe, faint thin stripes running perpendicular to the long-period stripe are observed, as shown in Fig. 3(d). The periodic distance between the thin stripes is approximately 0.4 nm. We call these thin stripes as short-period stripes.

Figure 4 shows the STM images obtained from Fe films with an Fe coverage of 1.7 ML. It is observed that about 67% surface is covered by the second-layer Fe and about 4% surface is covered by the third-layer Fe, as shown in Fig. 4(a), where the second monolayer Fe film is outlined by dotted lines. In the corresponding LEED pattern shown in Fig. 4(b), three additional satellite spots appear around the first-order spots of the substrate, forming clear triangular patterns, as indicated by A, B, and C. The spot A is superimposed on a first-order spot of the substrate, as indicated in the discussion. We have also collected the LEED pattern at off normal in order to focus around only one integral spot, and found that all three spots (A, B, and C) are circular spots, as shown in Fig. 4(c). In addition to the clear spots, very diffuse spots also appear around the specular beam, as indicated by the arrows D, E, and F. A schematic illustration of the LEED pattern is shown in Fig. 4(d), where the first-order spots of the substrate are connected by solid lines.

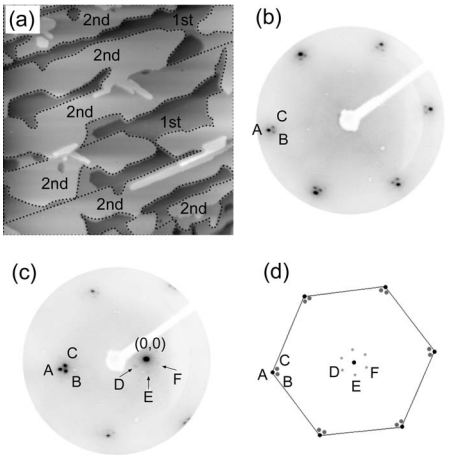

FIG. 4. STM images of Fe films grown on Ni(111) with Fe coverage of 1.7 ML. (a) Large-scale image (153×153 nm^2). (b) Corresponding LEED pattern (86 eV). (c) Corresponding LEED pattern collected at off normal (80 eV). (d) Schematic illustration of LEED pattern.

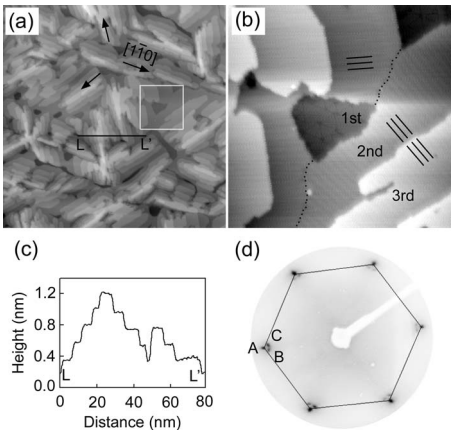

FIG. 5. STM images of Fe films grown on Ni(111) with Fe coverage of 3.2 ML. (a) Large-scale image (254×254 nm^2). (b) Magnified image (52×52 nm^2) of square area indicated in (a). (c) Cross-sectional line profile taken along line LL' in (a). (d) Corresponding LEED pattern (86 eV).

Figure 5 shows the STM images obtained from the Fe films with an Fe coverage of 3.2 ML. In the large-scale image shown in Fig. 5(a), the elongated islands oriented along three $\langle 1\bar{1}0\rangle$ directions are observed, as indicated by arrows. A magnified STM image of the square area outlined by white lines is shown in Fig. 5(b), where the Fe films from the first monolayer to the fourth monolayer are observed. The equilateral triangles and long-period stripes are still observed on the first and second monolayer Fe films, respectively. The stripes are indicated by parallel lines, and the domain boundary between two striped structures is indicated by dotted lines in the image. It is observed that the first and second monolayer Fe films grow almost completely over the substrate, whereas from the third monolayer onward, the Fe films grow on each elongated stripe domain to form the elongated islands. These elongated islands are stacked with 3–5 monatomic Fe layers, showing the ridgelike shapes. We have noted that the long-period stripes are also observable on the third monolayer Fe and even on the fourth monolayer Fe. The arrangement of the stripes on third Fe layer is same to that on second Fe layer, as indicated by the parallel lines in Fig. 5(b). No defects or distinct structures are found on these Fe layers besides the stripes. The cross-sectional line profile taken along the line LL', which is drawn across the elongated islands in Fig. 5(a), indicates a ridgelike structure stacked with six monatomic Fe layers, as shown in Fig. 5(c). The main LEED spots (A, B, and C) become slightly elongated, and the diffuse spots around the specular beam of the substrate become invisible, as shown in Fig. 5(d).

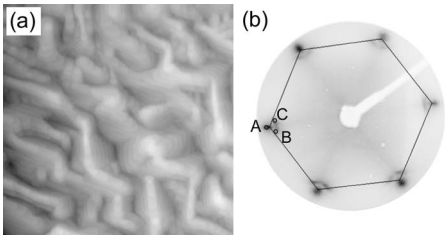

FIG. 6. STM images of Fe films grown on Ni(111) with Fe coverage of 4.2 ML. (a) Large-scale image (153×153 nm^2). (b) Corresponding LEED pattern (86 eV).

Figure 6 shows the STM images obtained from the Fe films with an Fe coverage of 4.2 ML. The elongated domains increase in number and become more irregular, as shown in Fig. 6(a). The main LEED spots (A, B, and C) become more elongated and the background becomes brighter, as shown in Fig. 6(b). It is noted that the triangle (ABC) become larger and the spot A is separated from the first-order spots of the substrate at this thickness.

IV. DISCUSSION

A. Misfit-induced vacancy defects

Triangular depression lines were frequently observed from ultrathin metal films, for example, a Au monolayer on Ni(111),[21] a Ag monolayer on Cu(111),[22,23] two Ag monolayers on Pt(111),[24] and two or three Co monolayers on Re(0001) alloyed with Co,[25] and were attributed to the dislocation loops formed in the first substrate layer[21–23] or the deposited adlayer[24,25] to relieve the strain caused by the lattice misfit between two different metals. For Au/Ni(111) (Ref. 21) and Ag/Cu(111) (Refs. 22 and 23) films, it was revealed by experiment[21,22] and theoretical calculation[21,23] that the lattice misfit-induced strain leads to the formation of vacancies in the first substrate layer and the subsequent shift of some substrate atoms from fcc to hcp sites within a triangular area. The boundary between the fcc and faulted hcp regions was a partial dislocation loop, which was observed as a depression line by STM.[21–23] For Ag/Pt(111) (Ref. 24) and Co/Re(0001) (Ref. 25) films, it was suggested that the stacking fault from fcc to hcp within a triangular area occurs in the surface layer of the deposited metal. The boundary between the fcc and hcp regions was also observed as a depression line by STM.[24,25] However, the triangular lines observed in this study differ from the dislocation loops mentioned above. The triangular lines of the Fe monolayer on Ni(111) consist of atomic-size dark spots, which are located in every second Ni atom site along the $\langle 1\bar{1}0\rangle$ direction and have a very small depth less than 0.03 nm [Figs. 2(b)–2(d)], whereas the triangular lines of dislocation loops are continued grooves.[21–25] Thus, we consider that the triangular lines of the Fe monolayer on Ni(111) cannot be attributed to dislocation loops. Also, the dark spots cannot be the Ni atoms segregated from the substrate into the Fe film or the atomic vacancies formed in the Fe film since they are not located in the hollow sites but in the Ni atom sites of the substrate surface. Considering the previous results indicating that the lattice misfit-induced strain creates atomic vacancies in the first substrate layer for Au/Ni(111) (Ref. 21) and Ag/Cu(111) (Refs. 22 and 23) films, we believe that the dark spots are related to the individual atomic vacancies formed in every second Ni atom site along the $\langle 1\bar{1}0\rangle$ direction in the first substrate layer in order to relieve the lattice misfit-induced strain. Because the interatomic distance of 0.254 nm in the fcc-Fe(111) plane is only about 2% larger than that of 0.249 nm in the Ni(111) plane, vacancies are few, and the lattice misfit-induced strain is relieved by adjusting the vacancy distribution, instead of shifting the atoms from fcc to hcp sites.[21–23]

B. Phase transition and growth mode

It has been well known that the epitaxial growth of a bcc metal on fcc(111) substrates leads to the formation of a bcc(110) phase with two possible in-plane orientation relationships, NW ($\langle 001\rangle_{bcc} \| \langle 1\bar{1}0\rangle_{fcc}$) and KS ($\langle 1\bar{1}1\rangle_{bcc} \| \langle 1\bar{1}0\rangle_{fcc}$), depending on the unit vector ratio ($r_{bcc/fcc}$) and layer-substrate interaction strength.[12] For the growth of Fe films on Ni(111), $r_{Fe/Ni}$ lies in a critical region, where neither NW nor KS energy curves have a minimum.[12] Previous experimental studies have shown that Fe grows pseudomorphically up to 2 (Ref. 17) or 3 (Refs. 13 and 18) ML and then transforms to the bcc(110) phase with the NW (Ref. 17) or KS (Refs. 13 and 18) orientation. However, the front of phase transition, the interface structure, and the growth mode could not be determined. In the present study, we have observed by STM that the three domains of the striped structure grow on the pseudomorphic fcc-Fe(111) layer, which grows two dimensionally on the Ni substrate. The striped structure tends to grow preferentially in the $\langle 1\bar{1}0\rangle$ direction, forming the elongated domains [Figs. 3(a) and 3(b)]. The stripes with a width of approximately 1.8 nm run perpendicular to the $\langle 1\bar{1}0\rangle$ direction. Along such long-period stripes, the short-period stripes with a period of 0.4 nm are observed [Fig. 3(d)]. At 1.7 ML coverage, about 67% surface is covered by the second-layer Fe, and only about 4% surface is covered by the third-layer Fe [Fig. 4(a)]. The corresponding LEED pattern shows the appearance of three additional satellite spots around each first-order spot of the substrate, forming a triangular pattern with one spot in the outer circle and two spots in the inner circle [A, B, and C in Figs. 4(b)–4(d)]. The spot A is superimposed on the main spot of the substrate. It has already been well discussed in the previous studies that these triangular satellite spots result from the epitaxial growth of bcc(110) films on fcc(111) with the NW orientation relationship.[4,18,26] The superimposition of the outer satellite and substrate spots indicates that the bcc lattice parameter is expanded in the $[1\bar{1}0]_{bcc}$ direction to make it equal to that of the substrate in the $[11\bar{2}]_{fcc}$ direction,[26] forming the one-dimensional NW_x orientation.[12] The threefold symmetry of the fcc(111) surface generates three equivalent domains in the NW_x orientation. Thus, we can attribute the three domains of the striped structure observed on the second monolayer Fe films to the distorted bcc(110) domains in the NW_x orientation. Figure 7 illustrates a distorted bcc(110) do-

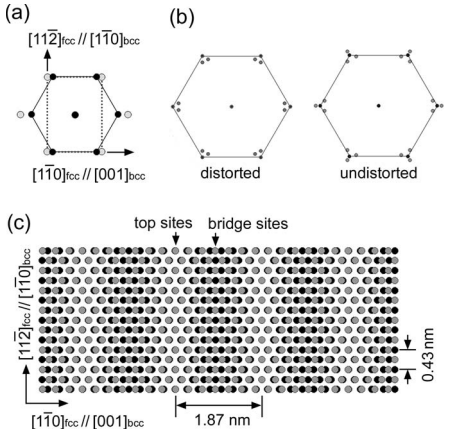

FIG. 7. Schematic illustration of bcc-Fe(110) domain on fcc-Fe(111) surface. (a) Orientation relationship between distorted bcc-Fe(110) domain (gray circles) and pseudomorphic fcc-Fe(111) (black circles) in one-dimensional NW_x model. (b) Simulated LEED patterns of distorted and undistorted bcc-Fe(110) domains in NW orientation. (c) Atomic arrangement of distorted bcc-Fe(110) monolayer on fcc-Fe(111).

main on the fcc(111) surface. The orientation relationship between the bcc-Fe(110) domain (gray circles) and the pseudomorphic fcc-Fe(111) (black circles) in the NW_x model is indicated in Fig. 7(a), where the $[001]_{bcc}$ direction is parallel to the $[1\bar{1}0]_{fcc}$ direction and the $[1\bar{1}0]_{bcc}$ direction is parallel to the $[11\bar{2}]_{fcc}$ direction. The bcc-Fe(110) lattice parameter is expanded by about 6.5% in the $[1\bar{1}0]_{bcc}$ direction to completely match it with the pseudomorphic fcc-Fe(111) lattice parameter in this direction, which results in the superimposition of the spot A and the substrate spot in the LEED pattern. We have simulated the LEED patterns for the distorted and undistorted bcc-Fe(110) domains in the NW orientation, using a simple geometrical LEED theory, as shown in Fig. 7(b). The simulated LEED pattern of the distorted bcc-Fe(110) domains agrees well with the experimental LEED pattern shown in Fig. 4 except the very diffuse spots around the specular beam. The diffuse spots may arise from the misfit-induced periodic superimposition of the bcc and fcc atoms along the $[001]_{bcc}$ direction, which forms parallel stripes with a width of 1.87 nm, as shown in Fig. 7(c). These parallel stripes appear as the long-period stripes with the period of about 1.8 nm in the STM images. The bcc atoms located in the top and quasitop sites appear raised relative to those located in the bridge sites. The periodicity of bcc atoms along the $[1\bar{1}0]_{bcc}$ direction is the same as that of the thin stripes observed on the long-period stripes, which may imply that the thin stripes arise from the periodicity of the bcc atoms in the $[1\bar{1}0]_{bcc}$ direction, though the atomic arrangement could not be identified by STM. We exclude the possibility that the second-layer atom lines along the $[001]_{bcc}$ direction reside between the first-layer atom lines as in the distorted fcc films grown on fcc(111) substrates[24,27] because the STM image of such distorted fcc films should not show the stripes observed in this study but the periodic line pairs reflecting the alternate stacking of the fcc and hcp regions along the $[1\bar{1}0]_{fcc}$ direction.[24,27] Since the lattice parameter of the distorted bcc(110) domain is expanded in the $[1\bar{1}0]_{bcc}$ direction to realize a complete NW_x epitaxy, the tensile stress is concentrated in this direction and the growth of the bcc(110) domain is limited to a small width in this direction, reducing the strain. Furthermore, these elongated bcc(110) domains with three different directions tend to grow alternately as observed in Fig. 3 because the boundaries between the stripe domains reduce the surface energy by allowing more isotropic strain relief.[28,29] The occurrence of the NW orientation is consistent with the result of Gazzadi *et al.*,[17] but not with that of D'Addato *et al.*[13] and Johnston *et al.*[18] D'Addato *et al.*[13] inferred the KS orientation of a bcc Fe structure grown on a Ni(111) single crystal from a LEED pattern. However, the poor quality and misorientation of their LEED pattern could not allow discrimination between KS and NW, and thus their conclusion was questionable.[17] Johnston *et al.*[18] observed the KS orientation of a bcc Fe structure grown on a 2 ML Ni/W(110) substrate by LEED and angle-resolved AES. This may be due to the nonideal structure of the Ni(111) substrate, which showed in-plane distortion and multidomains on W(110).[18]

With further deposition, the elongated domains of striped structure grow over the first monolayer Fe films and the thicker layers grow simultaneously on these elongated domains to form three-dimensional islands with elongated ridgelike shapes [Figs. 5(a) and 6(a)]. The number of layers in the growth front increases with the thickness of Fe and the striped structures are observed up to the fourth Fe layer. No defects, such as the triangles and dislocation lines, are observed on these Fe layers besides the stripes. The LEED spots A, B, and C become progressively elongated, and finally, the spot A is separated from the first-order spot of the substrate [Figs. 5(d) and 6(b)]. The main LEED spot observed from the Fe films of 4.2 ML is similar to the simulated LEED spots of the undistorted bcc(110) domains in the NW orientation shown in Fig. 7(b). Thus, we consider that the stripes formed in the second Fe layer remain for the Fe layers thicker than 3 ML. Kobayashi[30] has indicated by theoretical simulations that the lattice-mismatch-induced moiré patterns could be seen by STM even if they were buried deep in surface because the nanoscale waves propagate through many layers without decay. The origin of the stripes observed on the third and fourth Fe layers are not a new structure, but the stripes formed in the second Fe layer which propagate to the third and even fourth Fe layer surfaces as the lattice-mismatch-induced moiré patterns simulated by Kobayashi.[30] These results indicate that the first and second monolayer Fe films grow in an incomplete layer-by-layer growth mode and the thicker Fe films grow in a three-dimensional island growth mode. The distortion of the bcc(110) domains gradually decreases with increasing thickness, and the strain release occurs smoothly rather than through an abrupt transition, such as the formation of dislocations. This is in agreement with the previous findings obtained by angle-scanned PD indicating that the expanded interlayer spacing of bcc-Fe(110) on Ni(111) also gradually decreased to equilibrium values with increasing thickness.[17] We cannot identify whether the vacancies in the Ni substrate are removed by the growth of second or thicker Fe layers or

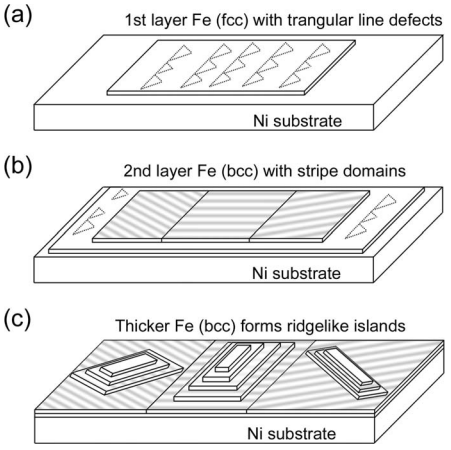

FIG. 8. Schematic illustration of Fe film growth on Ni(111). (a) Growth of first monolayer Fe film. (b) Growth of second monolayer Fe film. (c) Growth of thicker Fe films.

they are invisible from these thick Fe layer surfaces because STM is insensitive to such atomic-scale defect buried deep in surface.[30] On the basis of the above-mentioned experimental results and discussion, the Fe growth under the experimental conditions is illustrated in the overhead view, as shown in Fig. 8. In the initial deposition stage, a pseudomorphic fcc-Fe(111) monolayer grows on the Ni substrate and the misfit-induced atomic vacancies occur in the first layer of the Ni substrate, forming the triangular lines of dark spots on the surface, as shown in Fig. 8(a). With further deposition, the fcc(111) monolayer covers the substrate and the second monolayer Fe film composed of distorted bcc(110) domains grows on the first monolayer Fe film with the NW_x orientation, forming the alternate stripe domains on the surface, as shown in Fig. 8(b). Further deposition leads to the covering of the second monolayer Fe film on the first monolayer Fe film and the growth of thicker bcc (110) films on the distorted bcc(110) domains, forming the ridgelike islands, as shown in Fig. 8(c).

V. CONCLUSION

We have investigated the growth and structural transition of Fe thin films on Ni(111) at RT by combined LEED and STM. In the initial Fe deposition, a pseudomorphic fcc-Fe monolayer with triangular line defects grows from the step edge of the Ni substrate. Triangular lines consist of atomic-size dark spots, which are located in every second Ni atom site along the $\langle 1\bar{1}0\rangle_{\mathrm{fcc}}$ direction and have a small depth less than 0.03 nm. Thus, the dark spots are considered to be due to the atomic vacancies formed in the Ni substrate by the lattice misfit-induced strain. With further deposition, the second monolayer Fe film, which consists of three domains of a striped structure, grows on the first monolayer fcc-Fe film. The stripes with a width of approximately 1.8 nm run perpendicular to the $\langle 1\bar{1}0\rangle_{\mathrm{fcc}}$ direction and are explained in terms of the epitaxial growth of a distorted bcc-Fe(110) domain with a one-dimensional NW_x orientation. The lattice parameter of the bcc-Fe(110) domain is expanded by about 6.5% in the $[1\bar{1}0]_{\mathrm{bcc}}$ direction to completely match it with that of the pseudomorphic fcc-Fe(111) in this direction, and thus, the growth of the bcc-Fe(110) domain is limited to a small width in the $[1\bar{1}0]_{\mathrm{bcc}}$ direction, reducing the strain. Furthermore, these elongated bcc(110) domains tend to grow alternately to reduce the surface energy by allowing more isotropic strain relief. Further deposition leads to the growth of thicker bcc (110) films on the distorted bcc(110) domains, forming three-dimensional ridgelike islands. The distortion of the bcc(110) domains gradually decreases with increasing thickness, and the strain release occurs gradually rather than through an abrupt transition, such as the formation of dislocations. It is observed that the first and second monolayer Fe films grow in an incomplete layer-by-layer growth mode and the thicker Fe films grow in a three-dimensional island growth mode.

[1] V. L. Moruzzi, P. M. Marcus, K. Schwarz, and P. Mohn, Phys. Rev. B **34**, 1784 (1986).
[2] S. H. Lu, J. Quinn, D. Tian, and F. Jona, Surf. Sci. **209**, 364 (1989).
[3] V. L. Moruzzi, P. M. Marcus, and J. Kübler, Phys. Rev. B **39**, 6957 (1989).
[4] M. T. Kief and W. F. Egelhoff, Jr., Phys. Rev. B **47**, 10785 (1993).
[5] A. Brodde, K. Dreps, J. Binder, Ch. Lunau, and H. Neddermeyer, Phys. Rev. B **47**, 6609 (1993).
[6] A. Theobald, O. Schaff, C. J. Hirschmugl, V. Fernandez, K.-M. Schindler, M. Polcik, A. M. Bradshaw, and D. P. Woodruff, Phys. Rev. B **59**, 2313 (1999).
[7] A. Biedermann, M. Schmid, and P. Varga, Phys. Rev. Lett. **86**, 464 (2001).
[8] W. L. O'Brien and B. P. Tonner, Phys. Rev. B **52**, 15332 (1995).
[9] A. Biedermann, R. Tscheließnig, M. Schmid, and P. Varga, Phys. Rev. Lett. **87**, 086103 (2001).
[10] A. Biedermann, R. Tscheließnig, M. Schmid, and P. Varga, Appl. Phys. A: Mater. Sci. Process. **78**, 807 (2004).
[11] A. Biedermann, W. Rupp, M. Schmid, and P. Varga, Phys. Rev. B **73**, 165418 (2006).
[12] E. Bauer and J. H. van der Merwe, Phys. Rev. B **33**, 3657 (1986).
[13] S. D'Addato, L. Pasquali, G. C. Gazzadi, R. Verucchi, R. Capelli, and S. Nannarone, Surf. Sci. **454-456**, 692 (2000).
[14] R. Wu and A. J. Freeman, Phys. Rev. B **45**, 7205 (1992).
[15] P. Luches, G. C. Gazzadi, A. di Bona, L. Marassi, L. Pasquali, S. Valeri, and S. Nannarone, Surf. Sci. **419**, 207 (1999).
[16] G. C. Gazzadi, P. Luches, A. di Bona, L. Marassi, L. Pasquali, S. Valeri, and S. Nannarone, Phys. Rev. B **61**, 2246 (2000).
[17] G. C. Gazzadi, F. Bruno, R. Capelli, L. Pasquali, and S. Nannarone, Phys. Rev. B **65**, 205417 (2002).
[18] H. L. Johnston, C. S. Arnold, and D. Venus, Phys. Rev. B **55**,

13221 (1997).
[19] D. Sander, A. Enders, C. Schmidthals, J. Kirschner, H. L. Johnston, C. S. Arnold, and D. Venus, J. Appl. Phys. **81**, 4702 (1997).
[20] B. An, L. Zhang, S. Fukuyama, and K. Yokogawa, Jpn. J. Appl. Phys., Part 1 **46**, 5586 (2007).
[21] J. Jacobsen, L. P. Nielsen, F. Besenbacher, I. Stensgaard, E. Lægsgaard, T. Rasmussen, K. W. Jacobsen, and J. K. Nørskov, Phys. Rev. Lett. **75**, 489 (1995).
[22] K. Umezawa, S. Nakanishi, M. Yoshimura, K. Ojima, K. Ueda, and W. M. Gibson, Phys. Rev. B **63**, 035402 (2000).
[23] I. Meunier, G. Tréglia, J. M. Gay, B. Aufray, and B. Legrand, Phys. Rev. B **59**, 10910 (1999).
[24] H. Brune, H. Röder, C. Boragno, and K. Kern, Phys. Rev. B **49**, 2997 (1994).
[25] M. Parschau and K. Christmann, Surf. Sci. **423**, 303 (1999).
[26] F. Scheurer, P. Ohresser, H. Bulou, J. P. Deville, B. Carrière, and A. Dobroiu, Phys. Rev. B **56**, 13490 (1997).
[27] G. O. Pötschke and R. J. Behm, Phys. Rev. B **44**, 1442 (1991).
[28] O. L. Alerhand, D. Vanderbilt, R. D. Meade, and J. D. Joannopoulos, Phys. Rev. Lett. **61**, 1973 (1988).
[29] S. Narasimhan and D. Vanderbilt, Phys. Rev. Lett. **69**, 1564 (1992).
[30] K. Kobayashi, Phys. Rev. B **53**, 11091 (1996).